

Super-Resolution Imaging

Zitierweise:

Internationale Ausgabe: doi.org/10.1002/anie.202007878

Deutsche Ausgabe: doi.org/10.1002/ange.202007878

Multiple-Color Platinum Complex with Super-Large Stokes Shift for Super-Resolution Imaging of Autolysosome Escape

Liu-Yi Liu⁺, Hongbao Fang⁺, Qixin Chen⁺, Michael Ho-Yeung Chan⁺, Maggie Ng, Kang-Nan Wang, Wenting Liu, Zhiqi Tian, Jiajie Diao,* Zong-Wan Mao* und Vivian Wing-Wah Yam*

Abstract: It is of great significance to track the platinum drugs in real time with super-resolution to elucidate their mechanism of action, such as their behavior and distribution in live cells. Such information is required for further drug development. However, it is always challenging to design platinum complexes suitable for such research. Herein, we design a luminescent building block (**L**) for metal complexes and a dinuclear platinum complex (**Pt₂L**) for super-resolution imaging. Because of its super-large Stokes shift and excellent photophysical properties, **Pt₂L** is capable of serving as an ideal candidate for super-resolution imaging with extremely low luminescence background and high photobleaching resistance. Moreover, upon light stimulation, a matter flux of **Pt₂L** escaping from autolysosomes to nucleus was observed, which represents a new transportation path. Utilizing the photoactivated escape properties, we can regulate the nuclear accessibility of **Pt₂L** form autolysosomes with photo-selectivity, which provides a new way to improve the targeting of platinum drugs.

Introduction

Since 1978, cisplatin, a member of the platinum-based antineoplastic medications, has been approved as a clinical anticancer drug by FDA. Cisplatin and its analogues have been widely used as effective clinical chemotherapeutic drugs

for the treatment of cancer, such as ovarian cancer and prostate cancer.^[1] Meanwhile, various kinds of multifunctional platinum drugs have been developed.^[2] However, the side effects of platinum drugs (e.g., ototoxicity and nephrotoxicity) resulting from their poor tumor targeting limit their clinical effect.^[3] Currently, different approaches have been developed to improve tumor specificity of platinum drugs to mitigate their side effects, including modification of targeting groups or nanoparticles through active/passive targeting drug delivery, oxidation of bivalent platinum to non-toxic tetravalent platinum prodrugs and combination therapy.^[4] Previously, He and his colleagues^[5] exploited a Pt^{II} drug that enters lysosomes via endocytosis and can be isolated in the cytoplasm, so as to avoid toxicity and side effects. By light activation, the Pt^{II} drug escapes from the lysosome to the nucleus and attacks DNA to specifically kill the tumor cells. In addition to lysosomes, autolysosomes can also sequester drugs in the cytoplasm, which can provide additional avenues for platinum drugs silencing as prodrug to mitigate their side effects.^[6] To address the side effects of platinum drugs, a more detailed study of their mechanism of action, such as their behavior and distribution in live cells, is required. Although great progress has been made in understanding intracellular behavior of platinum drugs, the commonly used visualization of intracellular platinum drugs are currently all using confocal microscopy, and thus it is difficult to achieve dynamic tracking of ultrafine structure.^[7] Much is still unclear about the intracellular behavior and distribution of platinum drugs, which impede the development of platinum drugs.^[8] Therefore, it is of great significance to track the platinum drugs in real time with super-resolution to elucidate their dynamic behavior in live cells for drug development.

Cell imaging combined with platinum sensor or luminescent tag is a powerful method for non-invasively tracking platinum drugs in live cells. Among different microscopies for cell imaging, super-resolution microscopy provides a super-resolution imaging technique to break the optical diffraction limit, and realizes the super-resolution monitoring of the dynamic changes of organelles and drugs screening.^[9] Among them, super-resolution microscopy based on SIM (Structured Illumination Microscopy) is favored by researchers because of its advantages such as wavelength diversity, fast imaging and simple sample preparation.^[10] It has been widely used for organelle interaction, organoids imaging, drug screening and so on.^[11] However, it has always been a challenge to image platinum complexes directly in vivo, in real time and with subcellular resolution, because it is difficult to design luminescent platinum complexes for such imaging, which requires

[*] L.-Y. Liu,^[†] Dr. K.-N. Wang, Dr. W. Liu, Prof. Dr. Z.-W. Mao, Prof. Dr. V. W.-W. Yam
MOE Key Laboratory of Bioinorganic and Synthetic Chemistry, School of Chemistry, Sun Yat-Sen University
Guangzhou 510275 (P. R. China)
E-Mail: cesmzw@mail.sysu.edu.cn

H. Fang,^[†] Z. Tian, Prof. Dr. J. Diao
Department of Cancer Biology, University of Cincinnati College of Medicine
Cincinnati, OH 45267 (USA)
E-Mail: jiajie.diao@uc.edu

Dr. Q. Chen^[†]
Institute of Materia Medica, Shandong First Medical University and Shandong Academy of Medical Sciences
Jinan 250062 (P. R. China)

Dr. M. H.-Y. Chan,^[†] Dr. M. Ng, Prof. Dr. V. W.-W. Yam
Institute of Molecular Functional Materials and Department of Chemistry, The University of Hong Kong
Pokfulam Road, Hong Kong (P. R. China)
E-Mail: wwyam@hku.hk

[†] These authors contributed equally to this work.

 Supporting information and the ORCID identification number(s) for the author(s) of this article can be found under:
 <https://doi.org/10.1002/anie.202007878>.

not only good cell permeability, but also better optical properties of probes to meet the resolution, such as brighter luminescence and lower luminescence background.^[12] Thus, the rational design of platinum complexes for super-resolution imaging is critical. The large Stokes shift design of the probe can effectively reduce the background interference by reducing the overlap between excitation light and emitted light. However, to date, there are few luminescent compounds containing platinum complex motifs with super-large Stokes shift,^[13] and there is a lack of design guidance for these platinum complexes.^[8,14] Indeed, it is urgently needed to rationally design and provide design guidance of platinum complexes with super-large Stokes shift for super-resolution imaging to study the dynamic changes and metabolic processes of platinum complexes in cells with super-resolution.

In general, the platinum complexes with amine-type N coordination do not show fluorescence or phosphorescence, and therefore it is difficult to directly track their dynamic processes in live cells. Herein, we have designed a tripodal luminescent ligand, **L** (2-(4-(bis(4-(pyridin-4-yl)phenyl)amino)styryl)-1-methylquinolin-1-ium iodide), as a building block for platinum complexes. Through coordination of platinum moiety **Pt(dien)** (dien: diethylenetriamine) on two pyridine groups of **L**, a dinuclear platinum complex, **Pt₂L** ([Pt(dien)₂L](NO₃)₅), was obtained. The photophysical properties of **Pt₂L** and **L** were investigated in detail to analyze the effect of the coordination of platinum moiety on the photophysical properties of **L** for further design. Due to its super-large Stokes shift and excellent photophysical properties, **Pt₂L** can achieve super-resolution imaging with an extremely low luminescence background and shows a high photobleaching resistance. Furthermore, we have tracked the photoactivated escape of **Pt₂L** from autolysosomes to nucleus in live cells with super-resolution. **Pt₂L** can be isolated in autolysosomes, and then specifically escapes to nucleus and interacts with DNA including duplex and G-quadruplex DNA via photo-selectivity, showing the potential as photoactivated prodrug and providing a new way to reduce the side effects of platinum drugs.

Results and Discussion

Design and Synthesis

D- π -A type molecules, which are composed of electron-donating (D) and electron-accepting (A) units connected by π -bridge, are highly modifiable to achieve rich photophysical properties and other desired properties.^[15] As shown in Scheme S1, we designed a tripodal D- π -A type ligand **L** by connecting a quinolinium moiety (A) and a triphenylamine derivative moiety (D) with a carbon-carbon double bond (π -bridge). In this tripodal structure of **L** with triphenylamine at the center, one arm connects to quinolinium by a double bond for luminescence and the other two arms connect to pyridine by a single bond for the coordination with platinum moiety. By coordinating **Pt(dien)** (a hydrophilic platinum unit with two positive charges) on the two pyridine groups of **L**, the dinuclear platinum complex, **Pt₂L** (Figure 1a), with better

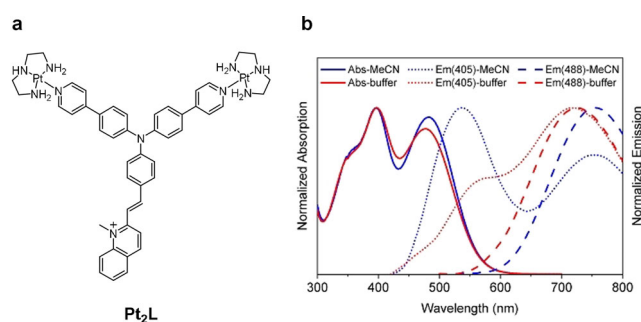


Figure 1. a) Chemical structure of **Pt₂L**. b) UV/Vis absorption and emission spectra of **Pt₂L** (10 μ M) measured in acetonitrile and tris-HCl buffer (10 mM, pH 7.4, 100 mM K⁺) with excitation at $\lambda_{\text{ex}} = 405$ nm and $\lambda_{\text{ex}} = 488$ nm.

water solubility and better affinity to negatively charged DNA, was obtained.^[16] The compounds **L** and **Pt₂L** were thoroughly characterized by ¹H NMR, ¹³C NMR, elemental analysis and mass spectrometry (Figure S1-S5).

Photophysical Properties

To facilitate the spectroscopic assignment of **Pt₂L**, an investigation into the photophysical properties of **L** has been conducted. **L** is found to display a high-energy absorption band at ≈ 355 nm and a low-energy absorption band at ≈ 500 nm in solution (Figure S6). The high-energy absorption band is found to be relatively insensitive to the change in solvent polarity and is characteristic of the π - π^* transition of the triphenylamine moiety.^[17] Moreover, the low-energy absorption band is found to display a blue shift upon increasing solvent polarity, which can be well-fitted to the plot of Dimroth's solvent parameter (Figure S7), suggesting the charge transfer character of the transition. **Pt₂L** shows a similar absorption profile when compared to that of **L**, exhibiting a high-energy absorption band at ≈ 400 nm and a low-energy absorption band at ≈ 490 nm in acetonitrile solution (Figure 1b). The high-energy band is found to show a red shift when compared to that of **L**, and is assigned as a metal-perturbed π - π^* transition of the triphenylamine moiety. Comparing the low-energy absorption band of **Pt₂L** and **L**, the shift of the absorption maxima is found to be small, suggesting the insignificant contribution of the metal center towards this low-energy transition. The low-energy absorption bands in **L** and **Pt₂L** are tentatively assigned as an intramolecular charge transfer (ICT) transition and an intraligand charge transfer (ILCT) transition, respectively, from the electron-donating triphenylamine moiety to the electron-accepting quinolinium moiety.

The emissive properties of **Pt₂L** have been investigated. Interestingly, two emission bands at ≈ 530 nm and ≈ 700 nm are observed upon excitation at $\lambda_{\text{ex}} = 405$ nm, while only one emission band at ≈ 700 nm is observed upon excitation at $\lambda_{\text{ex}} = 488$ nm (Figure 1b). From the differences in the excitation spectra of these two emission bands, it is believed that they are of different emission origin (Figure S8). This is further supported by the differences in the lifetimes of their



emissive excited states, in which the high-energy emission band at ≈ 530 nm shows an excited state lifetime of 10.8 μ s while that of the low-energy emission band at ≈ 700 nm shows an excited state lifetime of 0.16 μ s. Thus, the high-energy emission band at ≈ 530 nm is tentatively assigned as originated from a triplet metal-perturbed intraligand ^3IL excited state, as suggested by the relatively long excited-state lifetime. The low-energy emission band at ≈ 700 nm shows responsive behavior to solvent polarity (Figure S9) and is suggestive of its charge transfer excited state character. Thus, this low-energy emission band is assigned as originated from a triplet metal-perturbed intraligand charge transfer $^3\text{ILCT}$ [$\pi(\text{triphenylamine}) \rightarrow \pi^*(\text{quinolinium})$] excited state. On the other hand, a low-energy emission band at ≈ 800 nm is observed in the acetonitrile solution of **L** (Figure S6). A comparison of the low-energy emission bands between **L** and **Pt₂L** in acetonitrile solutions reveals a blue shift in the emission band upon the coordination of the platinum(II) centers. Such an observation can be attributed to the stabilization of the $\pi(\text{triphenylamine})$ orbital upon coordination of two positively-charged platinum(II) centers, reducing the electron-donating strength of triphenylamine, which further corroborates the metal-perturbed $^3\text{ILCT}$ emission assignment.

Computational Study

To investigate the nature of the absorption origins of **L** and **Pt₂L** and that of the emission origin of **Pt₂L**, density functional theory (DFT) and time-dependent DFT (TDDFT) calculations have been performed. The ground-state geometries of **L** and **Pt₂L** optimized in acetonitrile with the hybrid B3LYP functional using the Coulomb-attenuating method (CAM-B3LYP), which combines the hybrid qualities of B3LYP and the long-range correction, are shown in Figure S10. The simulated UV-vis spectra of **L** and **Pt₂L** are shown in Figures S11, S12. Their first ten singlet-singlet transitions computed by the TDDFT/CPCM (CH_3CN) method are summarized in Table S1, and selected molecular orbitals involved in the transitions are depicted in Figures S13, S14. For both **L** and **Pt₂L**, the low-energy absorption bands computed at 432 and 416 nm, respectively, are contributed by the HOMO \rightarrow LUMO excitation. The HOMO is predominantly the π orbital localized on the triphenylamine moiety, whereas the LUMO is the π^* orbital mainly localized on the quinolinium moiety. Therefore, the low-energy absorption bands in **L** and **Pt₂L** can be assigned as ICT and ILCT, respectively, from the triphenylamine moiety to the quinolinium moiety. The high-energy absorption band of **L** computed at 305 nm is contributed by the HOMO \rightarrow LUMO + 2 excitation, where the LUMO + 2 is the π^* orbital on the triphenylamine moiety. As a result, the high-energy absorption band of **L** can be assigned as $\pi \rightarrow \pi^*$ transition of the triphenylamine moiety. Similarly, the high-energy absorption band of **Pt₂L** computed at 341 nm is attributed to the HOMO \rightarrow LUMO + 1 excitation, where LUMO + 1 is the π^* orbital on the triphenylamine moiety. Therefore, the high-energy absorption band of **Pt₂L** is assigned as $\pi \rightarrow \pi^*$ transition of the triphenylamine moiety.

To further investigate the nature of the emissive state, geometry optimization on the lowest-lying triplet excited state (T_1) of **Pt₂L** has been performed with the unrestricted formalism, namely, UCAM-B3LYP/CPCM (CH_3CN). The emission wavelength of **Pt₂L** approximated by the energy difference between the S_0 and T_1 states at their corresponding optimized geometries has a value of 660 nm. Figure 2 shown are the optimized S_0 and T_1 geometries, and the spin density of the T_1 state of **Pt₂L**. The T_1 geometry is distorted from the S_0 geometry, with a dihedral angle C(1)-C(2)-C(3)-C(4) of 10.6°, which is much smaller than that in the S_0 geometry (31.5°). Moreover, the computed dipole moments of the S_0 and T_1 states are 19.6 and 41.2 Debye, respectively. The enhanced coplanarity of the phenyl ring with the quinolinium moiety in the T_1 geometry and the subsequent enhancement in the dipole moment from the S_0 state to the T_1 state are believed to be responsible for the super-large Stokes shift [calc.: from 416 to 660 nm (8900 cm^{-1}); expt.: from ≈ 490 to 750 nm (7100 cm^{-1})]; such Stokes shifts are comparable to those of the literature compounds described with super-large Stokes shift properties.^[15d] The spin density is predominantly localized on the triphenylamine and the quinolinium moieties,

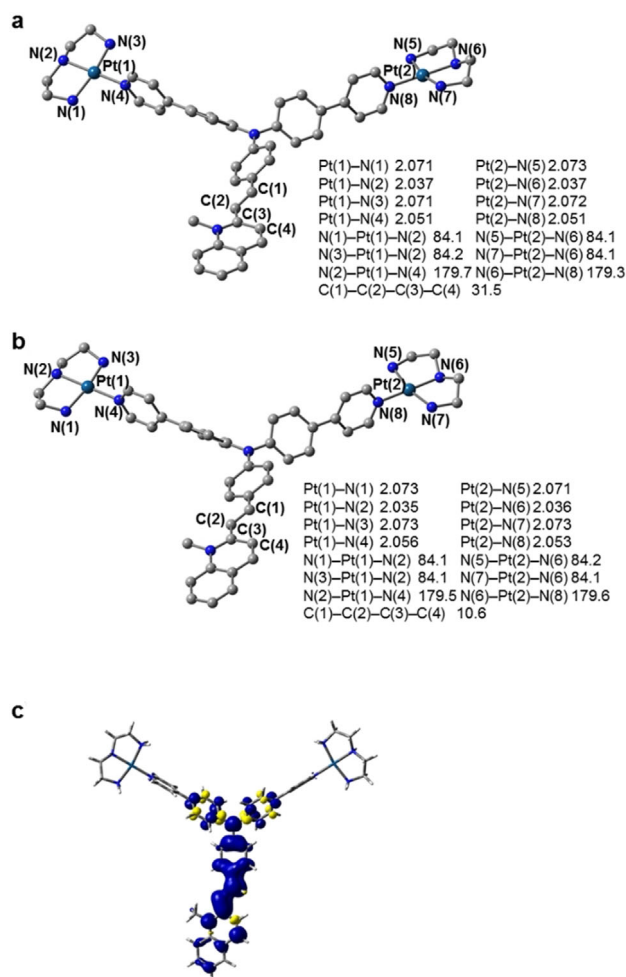


Figure 2. Optimized geometries of a) the ground state (S_0) and b) the T_1 state of **Pt₂L**, and c) the plot of spin density (isovalue = 0.002) of the T_1 state of **Pt₂L** at the optimized CAM-B3LYP geometry.

supporting the $^3\text{ILCT}$ character for the low-energy emission band at ≈ 700 nm. The theoretical study of Pt_2L and L elucidates the rational design of L as a luminescent building block of platinum complexes, and rationalizes the multiple-color and super-large Stokes shift of Pt_2L for further research.

Excellent Ability of Pt_2L for Super-Resolution Imaging with Low Background and High Photobleaching Resistance

In view of its excellent photophysical properties, Pt_2L is an excellent candidate for super-resolution imaging. To test the resolution limit of Pt_2L , HeLa cells were stained with Pt_2L for 12 h and then SIM imaging was performed. As shown in Figure 3, we randomly selected the SIM image, underlined where there was luminescence in the images (Figure 3a,b)

and observed the change of online intensity (Figure 3c). The FWHMs (full width at half maximum) of these bright puncta are about 200 nm, which breaks the traditional diffraction limit and realizes super-resolution imaging. It is helpful to observe the hyperfine structure of the stained cells of Pt_2L .

Because Pt_2L has a large Stokes shift [260 nm (7100 cm^{-1})], it can effectively avoid the background noise caused by excited light. To illustrate this advantage, we chose the commercial lysosomal dye LTR for comparison. The SIM images of cells co-stained with LTR and Pt_2L under different excitations are shown in Figure 3d and g. Then we randomly selected the background of two different regions in each image and made a luminescence intensity distribution map (Figure 3e,f and h,i). From these results, it can be seen that the background luminescence of SIM images of LTR was significantly higher than that of Pt_2L under the same condi-

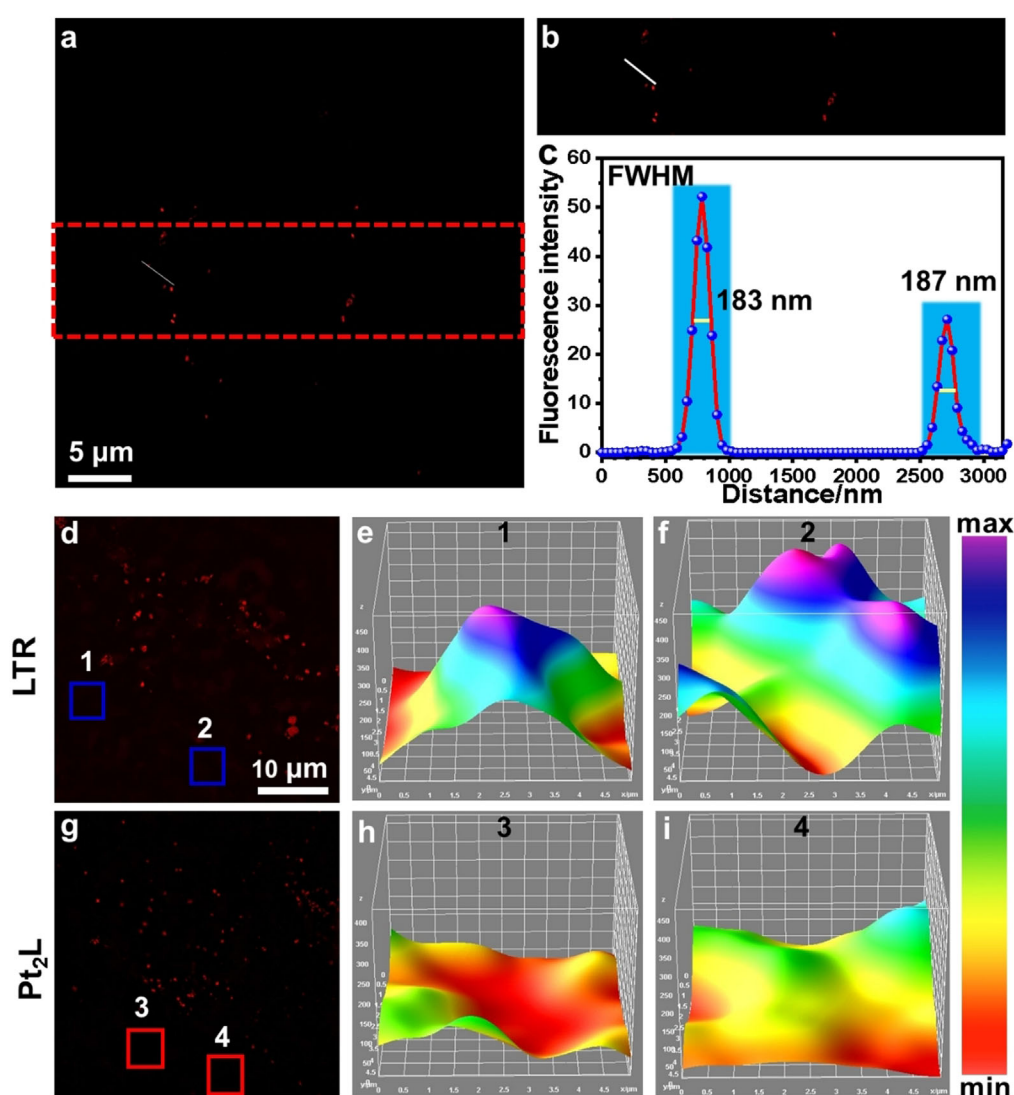


Figure 3. The resolution limit and background of SIM imaging with Pt_2L . a) The super-resolution imaging of HeLa cells stained by Pt_2L , $\lambda_{\text{ex}}=405$ nm, $\lambda_{\text{em}}=603$ nm. b) The local images from (a) in the red dotted box. c) The intensity profile of the white line in (b). Full width at half maximum (FWHM) indicates that the super-resolution imaging has been achieved. d) The super-resolution imaging of HeLa cells stained by LTR. e),f) The 3D intensity plots of the rectangle of integration (ROI) 1,2 from (d), $\lambda_{\text{ex}}=568$ nm, $\lambda_{\text{em}}=603$ nm. g) The super-resolution imaging of HeLa cells stained by Pt_2L . h),i) The 3D intensity plots of the ROI 3,4 from (g), $\lambda_{\text{ex}}=405$ nm, $\lambda_{\text{em}}=603$ nm.

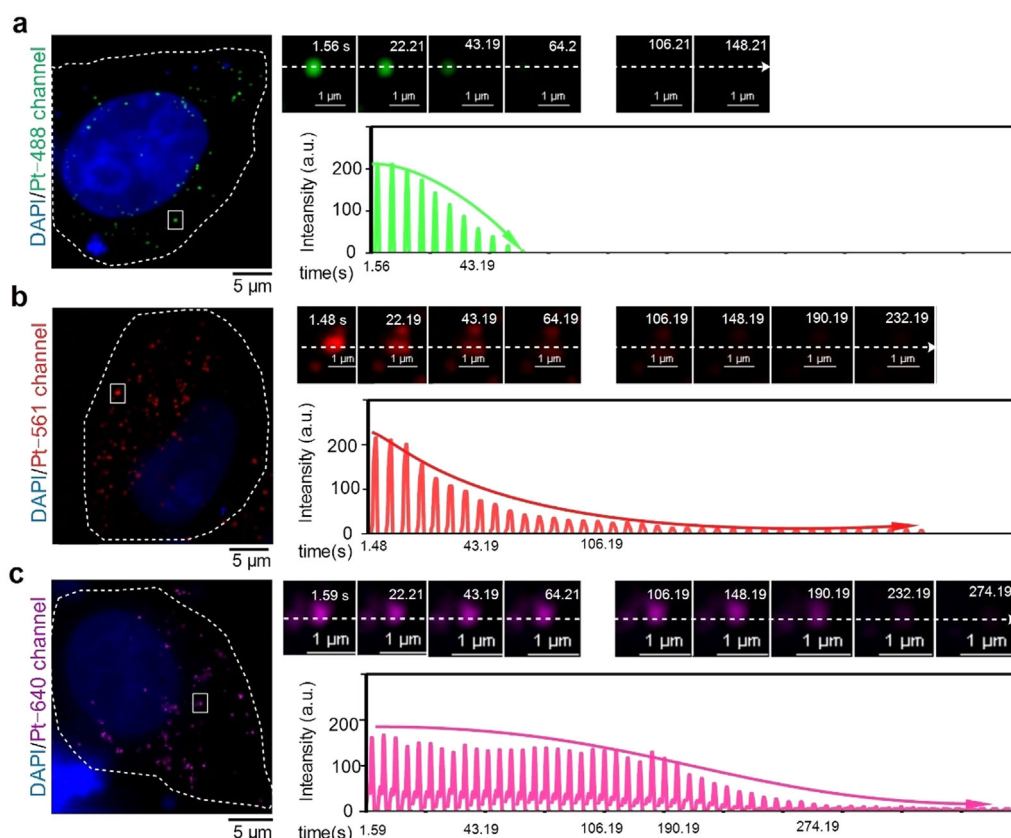


Figure 4. Photobleaching properties of Pt_2L for continuous imaging under a) 488-nm, b) 561-nm, and c) 640-nm lasers. White dotted lines indicate luminescence intensity shown in lower right of panel.

tions. This shows that Pt_2L not only can successfully achieve super-resolution imaging but also effectively improve the signal-to-noise ratio.

To characterize the photobleaching resistance of luminescence puncta stained by Pt_2L in three SIM laser channels (488, 561 and 640 nm), we co-stained HeLa cells with Pt_2L and DAPI and exposed them to continuous SIM laser illumination (Figure 4). The result showed that the luminescent particles stained by Pt_2L had high photobleaching resistance in both 561 nm and 640 nm channels, with a photobleaching lifetime of more than 108 s and 190 s, respectively. These results indicate that Pt_2L possesses excellent photostability and can be tracked for a long time in cells by super-resolution imaging.

Specific Recognition of Pt_2L to Autolysosomes in Live Cells

Considering that luminescence puncta stained by Pt_2L had luminescence in three channels under SIM, to determine which organelle Pt_2L could be located in, we took advantage of the fact that the luminescence quantum yield of the Pt-complex was much lower than that of commercial probes. We then set the exposure time to 10 ms and 6% laser intensity under SIM 561 nm channel. Under this condition, the particles stained by Pt_2L could not be imaged, whereas the commercial organelle-targeting probes could be imaged.

Next, we co-stained the cells with commercial endosome, autolysosome and lysosome probes, and found that Pt_2L and autolysosome probe had the highest overlap (Figure 5).

As it is generally accepted that autolysosomes do not engulf healthy mitochondria under normal conditions, to further verify the fact that our probes could label autolysosomes, we then use commercial mitochondrial probes (mitotracker green, MTG) and Pt_2L (Figure 5j–l) to co-stain cells. As expected, Pt_2L -labeled luminescent particles could not overlap with healthy mitochondria. This result further proves that Pt_2L could specifically label autolysosome in live cells. Pt_2L has the potential to study the dynamic autophagy level by specific recognition to autolysosomes through super-resolution imaging. Compared with confocal imaging, this provides an opportunity to track the ultrafine structure dynamics of autolysosomes.

Photoactivated Escape of Pt_2L from Autolysosomes to Nucleus

We found that after 5 min light irradiation, the luminescent particles stained by Pt_2L were located around the cell membrane with a high overlap under different SIM channels (488, 561 and 640 nm), whereas this event was reversed when the luminescent particles were located near the nucleus (Figure 6a,b). In addition, Pt_2L was found to gather on the nucleus after continuous light stimulation (Figure 6a). Simi-

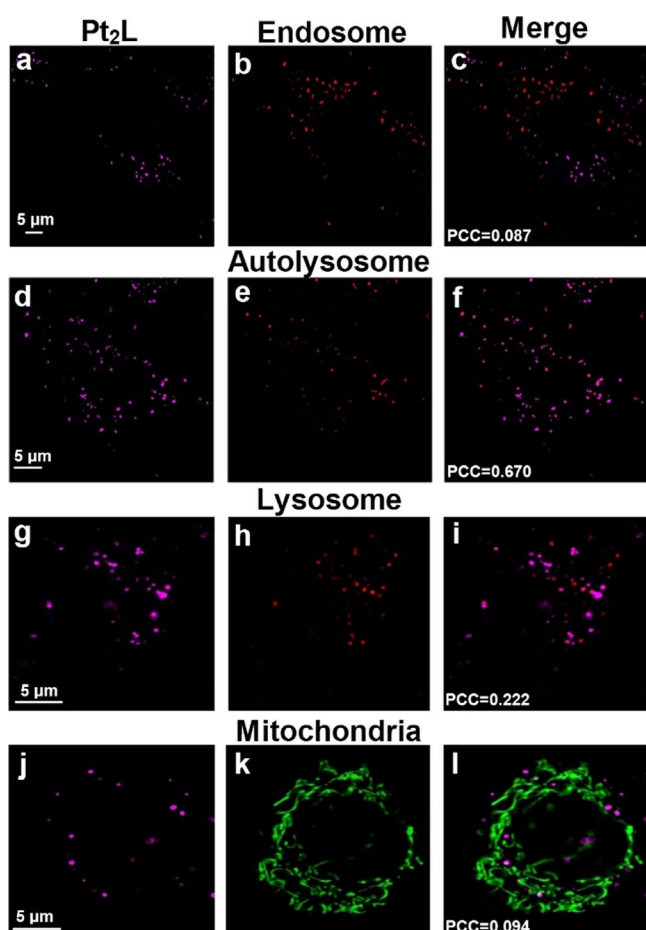


Figure 5. Co-localization of Pt_2L co-stained with a)–c) endosome, d)–f) autolysosome, g)–i) lysosome and j)–l) mitochondria under SIM 640 and 561 or 488 nm channels, and the co-localization coefficient (Pearson's correlation coefficient, PCC).

larly, we recorded a dynamic process in which the luminescence intensity of autolysosomes decreased gradually under continuous illumination of SIM 561 nm channel, while that of the nucleus increased gradually, indicating that Pt_2L escaped from autolysosomes to the nucleus (Figure 6c). To clarify the matrix material that Pt_2L binds in the nucleus, we then co-stained with DNA binding probe (DAPI) in light-stimulated cells (Figure 6d), and found that Pt_2L and DAPI had a high overlap (Figure 6e), indicating that Pt_2L could bind to nuclear DNA. As confirmed by the luminescence response of Pt_2L to DNA, the luminescence of Pt_2L increased obviously (115-fold for duplex DNA ds26 and 218-fold for G-quadruplex DNA 22AG) upon DNA binding. The binding constant (K_a) is calculated as $2.71 \pm 0.30 \times 10^6 \text{ M}^{-1}$ for ds26 and $1.10 \pm 0.18 \times 10^7 \text{ M}^{-1}$ for 22AG, indicating its high affinity to DNA (Figure S15). Pt_2L showed a high photoinduced singlet oxygen quantum yield ($\Phi_\Delta = 0.65$ for 425 nm irradiation and 0.95 for 525 nm irradiation; Figure S16), so the effect of reactive oxygen species (ROS) production by Pt_2L on its escape behavior was further studied. As shown in Figure S17, with the increase of irradiation time, the 2',7'-dichlorofluorescein (DCF) fluorescence increased and Pt_2L gradually escaped to the nucleus, which suggested that the escape behavior of Pt_2L

was associated with its ROS production and the damage of autolysosomes (Figure 6d), and was consistent with the reported mechanism.^[5,18] For the first time, we observed a new transportation path that a matter flux escapes from autolysosomes to nucleus upon light stimulation.

Pt_2L showed the behavior of photoactivated escaping from autolysosomes to nucleus and interacting with DNA, which had the potential of controllable nuclear accessibility and DNA binding with photo-selectivity to improve the treatment specificity for tumor.^[5,16] To validate this, the intracellular behavior and cytotoxicity of Pt_2L were further investigated. By observing the intracellular distribution of Pt_2L within 30 h, we found that Pt_2L can effectively enter the cytoplasm of living A549 cells in 2 h, and can remain in the cytoplasm for over 30 h without entering the nucleus (Figure S18). These results indicate that Pt_2L can be isolated in the cytoplasm and cannot enter the nucleus for a long time under dark conditions, and further demonstrate the selectivity of photoactivated nuclear accessibility. The cell uptake of Pt_2L in A549 cells was then performed under different incubation conditions in the dark. Compared with the control group (incubation at 37 °C), the luminescence intensity of Pt_2L in the low-temperature group (incubation at 4 °C) was decreased obviously, while that in the experimental group (preincubation with endocytosis inhibitor chloroquine) remained unchanged (Figure S19). These results suggest that Pt_2L enters the cell by energy-dependent non-endocytosis. Furthermore, Pt_2L possesses high singlet oxygen quantum yield and photoinduced ROS production ability, showing the potential to be used as a photodynamic therapy (PDT) photosensitizer in the treatment of tumors.^[19] So the dark and light cytotoxicity of Pt_2L were performed using MTT assay. The results showed that Pt_2L did not exhibit obvious cytotoxicity at the concentration of 0–12.5 μM for 48 h in the dark with the viability over 70% for all cell lines tested. As the concentration increased, Pt_2L showed some cytotoxicity to cells with IC_{50} about 141 μM for A549 cells and 33.9 μM for HeLa cells. With 425 nm and 525 nm photoirradiation (15 min, 40 mWcm^{-2} ; corresponding to the high-energy absorption band of Pt_2L at ≈ 400 nm and the low-energy absorption band at ≈ 490 nm), the IC_{50} values of A549 cells were about 3.3 and 2.4 μM , respectively, and those of HeLa cells were about 2.5 and 1.9 μM , respectively (Figure S20 and Table S5). The IC_{50} values upon 525 nm irradiation is slightly lower than that upon 425 nm irradiation, possibly due to the higher singlet oxygen quantum yield upon 525 nm irradiation (Figure S16). The light-induced cytotoxicity of Pt_2L is higher than that of cisplatin, and shows comparable phototoxicity to the reported photosensitizers for PDT.^[5,16a,18] These suggest that Pt_2L has significant photoactivated cytotoxicity, and can improve tumor specificity by selectively irradiating the tumor tissue for tumor treatment. Compared with the reported Pt-BDPA utilizing lysosome sequestration for platinum complex silencing as prodrug,^[5] we verified that autolysosomes also can be used for platinum complex sequestration, further opening up new ways for the design of this kind of platinum complexes. Since autophagy plays a very important role in tumor and shows environmentally dependent, the real-time

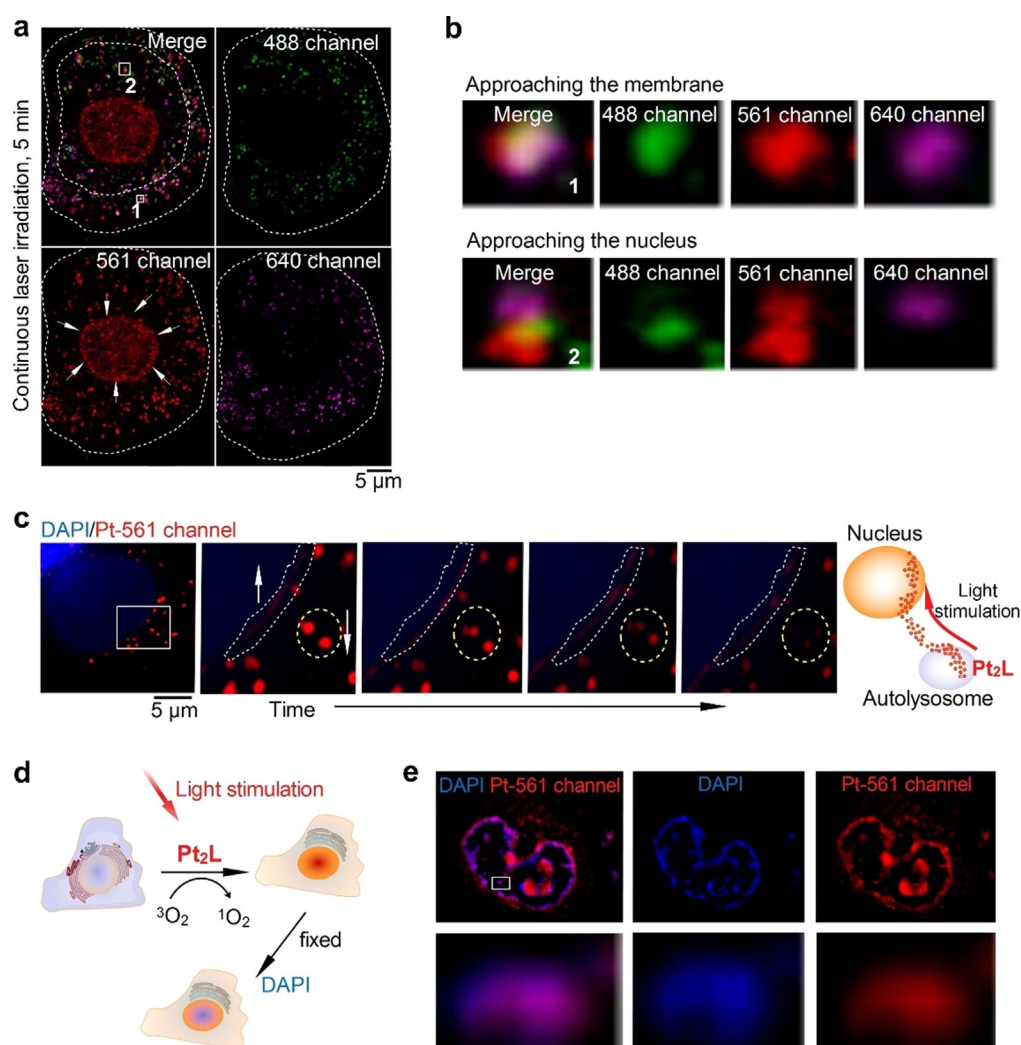


Figure 6. a) Co-localization of Pt₂L in different SIM channels (488, 561, and 640 nm) after laser stimulation for 5 min. b) Representative co-localization of Pt₂L in the white rectangles (1,2) of (a). c) The dynamics process of photoactivated Pt₂L escaping from the autolysosomes to the nucleus, with the luminescence intensity gradually decreasing in autolysosomes and increasing in nucleus. d) Schematic representation of co-localization of Pt₂L and DNA binding probe (DAPI) in fixed cells shown in (e).

tracking of autolysosomes by Pt₂L simultaneously allows us to detect the level of autophagy in cells to assist in diagnosis.

Conclusion

In summary, we designed a multiple-color platinum complex Pt₂L with super-large Stokes shift, which can be used for super-resolution imaging. On the technique side, due to its super-large Stokes shift and excellent photophysical properties, Pt₂L can achieve super-resolution imaging with an extremely low luminescence background and shows a high photobleaching resistance. On the biological side, our ability to study matter flux in live cells can be significantly enhanced by super-resolution imaging with Pt₂L. Under light stimulation, as a new transportation path, a matter flux escaping from autolysosomes to the nucleus was observed for the first time. By exploiting the photoactivated escape from autolysosomes to the nucleus, Pt₂L shows the potential to improve the

treatment specificity with photo-selectivity, providing a new way to reduce the side effects of platinum drugs. Our work provides building blocks (L) for the construction of platinum complexes, and provides design guidance of platinum complexes with excellent optical properties and super-large Stokes shift for the research of platinum complex behavior in vivo with super-resolution to promote the development of platinum drugs.

Acknowledgements

This work was funded by the National Science Foundation of China (Nos. 21837006 and 91953117), the Ministry of Education of China (IRT-17R111), and the Fundamental Research Funds for the Central Universities. V.W.-W.Y. acknowledges the support from the HKU University Research Committee (URC) Strategically Oriented Research Theme (SORT) on Functional Materials for Molecular Electronics

and the General Research Fund (GRF) grant from the Research Grants Council of the Hong Kong Special Administrative Region, People's Republic of China (HKU 17306219). Computations were performed using the HKU ITS research computing facilities. J.D. was supported by the Department of Cancer Biology, University of Cincinnati College of Medicine. Q.X.C. acknowledges the support from the Academic Promotion Program of Shandong First Medical University (No. 2019LJ003). We thank the Translational Medicine Core Facility of Shandong University for consultation and instrument availability that supported this work, and thank Ms. Jie Zhang for assistance with 3D-SIM microscopy.

Conflict of interest

The authors declare no conflict of interest.

Stichwörter: autolysosome · platinum complexes · real-time tracking · Stokes shift · super-resolution imaging

- [1] a) S. Dasari, P. B. Tchounwou, *Eur. J. Pharmacol.* **2014**, *740*, 364–378; b) P. M. Takahara, A. C. Rosenzweig, C. A. Frederick, S. J. Lippard, *Nature* **1995**, *377*, 649–652.
- [2] a) Q. Cheng, Y. Liu, *Wiley Interdiscip. Rev. Nanomed. Nanobiotechnol.* **2017**, *9*, e1410; b) Z. Zhu, X. Wang, T. Li, S. Aime, P. J. Sadler, Z. Guo, *Angew. Chem. Int. Ed.* **2014**, *53*, 13225–13228; *Angew. Chem.* **2014**, *126*, 13441–13444; c) S. Xu, X. Zhu, C. Zhang, W. Huang, Y. Zhou, D. Yan, *Nat. Commun.* **2018**, *9*, 2053.
- [3] a) R. Oun, Y. E. Moussa, N. J. Wheate, *Dalton Trans.* **2018**, *47*, 6645–6653; b) C. A. Rabik, M. E. Dolan, *Cancer Treat. Rev.* **2007**, *33*, 9–23.
- [4] T. C. Johnstone, K. Suntharalingam, S. J. Lippard, *Chem. Rev.* **2016**, *116*, 3436–3486.
- [5] X. Xue, C. Qian, H. Fang, H. K. Liu, H. Yuan, Z. Guo, Y. Bai, W. He, *Angew. Chem. Int. Ed.* **2019**, *58*, 12661–12666; *Angew. Chem.* **2019**, *131*, 12791–12796.
- [6] D. Denton, S. Kumar, *Cell Death Differ.* **2019**, *26*, 605–616.
- [7] a) X. Wang, X. Wang, S. Jin, N. Muhammad, Z. Guo, *Chem. Rev.* **2019**, *119*, 1138–1192; b) X. Wang, X. Wang, Z. Guo, *Acc. Chem. Res.* **2015**, *48*, 2622–2631; c) E. Baggaley, J. A. Weinstein, J. A. G. Williams, *Coord. Chem. Rev.* **2012**, *256*, 1762–1785; d) S. W. Botchway, M. Charnley, J. W. Haycock, A. W. Parker, D. L. Rochester, J. A. Weinstein, J. A. Williams, *Proc. Natl. Acad. Sci. USA* **2008**, *105*, 16071–16076; e) E. Baggaley, S. W. Botchway, J. W. Haycock, H. Morris, I. V. Sazanovich, J. A. G. Williams, J. A. Weinstein, *Chem. Sci.* **2014**, *5*, 879–886; f) X. Xue, C. Zhu, H. Chen, Y. Bai, X. Shi, Y. Jiao, Z. Chen, Y. Miao, W. He, Z. Guo, *Inorg. Chem.* **2017**, *56*, 3754–3762.
- [8] a) M. P. Tracey, D. Pham, K. Koide, *Chem. Soc. Rev.* **2015**, *44*, 4769–4791; b) N. J. Farrer, D. M. Griffith, *Curr. Opin. Chem. Biol.* **2020**, *55*, 59–68.
- [9] a) Q. Chen, C. Jin, X. Shao, R. Guan, Z. Tian, C. Wang, F. Liu, P. Ling, J. L. Guan, L. Ji, F. Wang, H. Chao, J. Diao, *Small* **2018**, *14*, 1802166; b) Q. Chen, X. Shao, Z. Tian, Y. Chen, P. Mondal, F. Liu, F. Wang, P. Ling, W. He, K. Zhang, Z. Guo, J. Diao, *Nano Res.* **2019**, *12*, 1009–1015; c) X. Shao, Q. Chen, L. Hu, Z. Tian, L. Liu, F. Liu, F. Wang, P. Ling, Z. W. Mao, J. Diao, *Nano Res.* **2020**, *13*, 2149–2155.
- [10] a) R. Heintzmann, T. Huser, *Chem. Rev.* **2017**, *117*, 13890–13908; b) Y. Wu, H. Shroff, *Nat. Methods* **2018**, *15*, 1011–1019.
- [11] a) H. Fang, S. Yao, Q. Chen, C. Liu, Y. Cai, S. Geng, Y. Bai, Z. Tian, A. L. Zacharias, T. Takebe, Y. Chen, Z. Guo, W. He, J. Diao, *ACS Nano* **2019**, *13*, 14426–14436; b) Q. Chen, X. Shao, M. Hao, H. Fang, R. Guan, Z. Tian, M. Li, C. Wang, L. Ji, H. Chao, J. L. Guan, J. Diao, *Biomaterials* **2020**, *250*, 120059; c) K. Qiu, Y. Du, J. Liu, J. L. Guan, H. Chao, J. Diao, *Theranostics* **2020**, *10*, 6072–6081.
- [12] L. Wang, M. Tran, E. D'Este, J. Roberti, B. Koch, L. Xue, K. Johnsson, *Nat. Chem.* **2020**, *12*, 165–172.
- [13] a) K. H.-Y. Chan, H.-S. Chow, K. M.-C. Wong, M. C.-L. Yeung, V. W.-W. Yam, *Chem. Sci.* **2010**, *1*, 477; b) C. Y.-S. Chung, S. P.-Y. Li, M.-W. Louie, K. K.-W. Lo, V. W.-W. Yam, *Chem. Sci.* **2013**, *4*, 2453; c) M. C.-L. Yeung, V. W.-W. Yam, *Chem. Sci.* **2013**, *4*, 2928; d) M. C.-L. Yeung, V. W.-W. Yam, *Chem. Soc. Rev.* **2015**, *44*, 4192–4202.
- [14] M. A. Miller, B. Askevold, K. S. Yang, R. H. Kohler, R. Weissleder, *ChemMedChem* **2014**, *9*, 1131–1135.
- [15] a) D. Wang, H. Su, R. T. K. Kwok, X. Hu, H. Zou, Q. Luo, M. S. Lee, W. Xu, J. W. Y. Lam, B. Z. Tang, *Chem. Sci.* **2018**, *9*, 3685–3693; b) K.-N. Wang, X.-J. Chao, B. Liu, D.-J. Zhou, L. He, X.-H. Zheng, Q. Cao, C.-P. Tan, C. Zhang, Z.-W. Mao, *Chem. Commun.* **2018**, *54*, 2635–2638; c) K.-N. Wang, Q. Cao, L.-Y. Liu, Z.-J. Zhao, W.-T. Liu, D.-J. Zhou, C. Tan, W. Xia, L. Ji, Z.-W. Mao, *Chem. Sci.* **2019**, *10*, 10053–10064; d) J. Hong, E. Zhou, S. Gong, G. Feng, *Dyes Pigm.* **2019**, *160*, 787–793.
- [16] a) Y.-F. Zhong, H. Zhang, W.-T. Liu, X.-H. Zheng, Y.-W. Zhou, Q. Cao, Y. Shen, Y. Zhao, P. Z. Qin, L.-N. Ji, Z.-W. Mao, *Chem. Eur. J.* **2017**, *23*, 16442–16446; b) W. Liu, Y.-F. Zhong, L.-Y. Liu, C.-T. Shen, W. Zeng, F. Wang, D. Yang, Z.-W. Mao, *Nat. Commun.* **2018**, *9*, 3496; c) L.-Y. Liu, W. Liu, K.-N. Wang, B.-C. Zhu, X.-Y. Xia, L.-N. Ji, Z.-W. Mao, *Angew. Chem. Int. Ed.* **2020**, *59*, 9719–9726; *Angew. Chem.* **2020**, *132*, 9806–9813.
- [17] a) Z. Ge, T. Hayakawa, S. Ando, M. Ueda, T. Akiike, H. Miyamoto, T. Kajita, M.-a. Kakimoto, *Adv. Funct. Mater.* **2008**, *18*, 584–590; b) Y. Tao, Q. Wang, Y. Shang, C. Yang, L. Ao, J. Qin, D. Ma, Z. Shuai, *Chem. Commun.* **2009**, 77–79; c) C.-Y. Chan, Y.-C. Wong, M.-Y. Chan, S.-H. Cheung, S.-K. So, V. W.-W. Yam, *Chem. Mater.* **2014**, *26*, 6585–6594.
- [18] H. Huang, B. Yu, P. Zhang, J. Huang, Y. Chen, G. Gasser, L. Ji, H. Chao, *Angew. Chem. Int. Ed.* **2015**, *54*, 14049–14052; *Angew. Chem.* **2015**, *127*, 14255–14258.
- [19] a) Z. Zhou, J. Liu, J. Huang, T. W. Rees, Y. Wang, H. Wang, X. Li, H. Chao, P. J. Stang, *Proc. Natl. Acad. Sci. USA* **2019**, *116*, 20296–20302; b) J. Karges, S. Kuang, F. Maschietto, O. Blacque, I. Ciofini, H. Chao, G. Gasser, *Nat. Commun.* **2020**, *11*, 3262–3262; c) A. Naik, R. Rubbiani, G. Gasser, B. Spingler, *Angew. Chem. Int. Ed.* **2014**, *53*, 6938–6941; *Angew. Chem.* **2014**, *126*, 7058–7061; d) Z. Deng, N. Wang, Y. Liu, Z. Xu, Z. Wang, T. C. Lau, G. Zhu, *J. Am. Chem. Soc.* **2020**, *142*, 7803–7812.

Manuskript erhalten: 2. Juni 2020

Akzeptierte Fassung online: 14. Juli 2020

Endgültige Fassung online: ■■ ■■ ■■■■

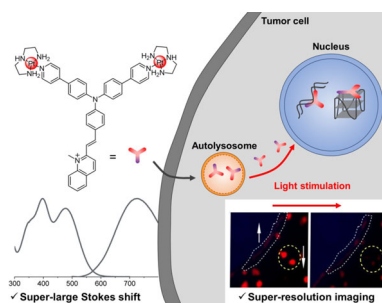
Forschungsartikel



Super-Resolution Imaging

L.-Y. Liu, H. Fang, Q. Chen, M. H.-Y. Chan,
M. Ng, K.-N. Wang, W. Liu, Z. Tian,
J. Diao,* Z.-W. Mao,*
V. W.-W. Yam*     

Multiple-Color Platinum Complex with
Super-Large Stokes Shift for Super-
Resolution Imaging of Autolysosome
Escape



A multiple-color platinum complex (Pt_2L) with super-large Stokes shift was designed for super-resolution imaging, showing an extremely low luminescence background and high photobleaching resistance. Moreover, upon light stimulation, a matter flux of Pt_2L escaping from autolysosomes to the nucleus is detected, which represents a new transportation path.

